Calculations of highfrequency response of twodimensional hot electrons in GaAs quantum wells

S. K. Sarkar, P. K. Ghosh, and D. Chattopadhyay

Citation: Journal of Applied Physics **78**, 283 (1995); doi: 10.1063/1.360671
View online: http://dx.doi.org/10.1063/1.360671
View Table of Contents: http://scitation.aip.org/content/aip/journal/jap/78/1?ver=pdfcov
Published by the AIP Publishing

Calculations of high-frequency response of two-dimensional hot electrons in GaAs quantum wells

S. K. Sarkar
Department of Electronics & Telecommunication, Bengal Engineering College (Deemed University), Howrah 711 103, India

P. K. Ghosh and D. Chattopadhyay
Institute of Radiophysics and Electronics 92, Acharya Prafulla Chandra Road, Calcutta 700 009, India

(Received 5 December 1994; accepted for publication 14 February 1995)

Small-signal ac mobility of two-dimensional (2D) degenerate hot electrons in a GaAs square quantum well is studied on a heated drifted Fermi–Dirac distribution function for the carriers. Carrier energy loss via longitudinal optic (LO) phonons, and the momenta losses via LO, acoustic and ionized impurity scatterings are considered. The ac mobility is found to drop off with frequency beyond 100 GHz although the drift velocity starts to lag behind the applied field at a lower frequency. The ac mobility μ_{ac} and the phase angle ϕ increase with the rise of the channel width and the 2D carrier concentration. However, the 3-dB cut-off frequency $f_{3\ dB}$ is found to decrease with increasing channel width. The values of μ_{ac} and $f_{3\ dB}$ are higher but those of ϕ are lower at 300 K than that at 77 K. © *1995 American Institute of Physics.*

I. INTRODUCTION

The two-dimensional (2D) transport of hot electrons in quantum wells (QWs) is the subject of many recent investigations.[1] As the QW thickness is comparable to the de Broglie wavelength, a subband structure is formed allowing 2D transport of carriers parallel to the interfacial planes. The reduction of the effects of ionized impurity scattering due to modulation doping enhances the carrier mobility, particularly at low temperatures where phonon scattering is suppressed.[2] Quantum structures, therefore, show promise for application in fast and high-frequency miniature devices.

As an aid to the device-related work and to understand the basic carrier kinetics, high-frequency transport of the 2D hot electrons in QW structures needs a careful investigation. In this article, we report calculations of the small-signal ac response of 2D hot electrons in a GaAs QW structure. The dependencies of the ac mobility on system parameters such as the 2D carrier concentration and the channel width are also studied.

II. THEORY

A GaAs QW of infinite barrier height is considered. This approximation is valid because the band offset between the well and the barrier layers is more than three times the average electron energy in the well for the dc electric field considered. The 2D carrier concentration (n_{2D}) and the channel width(L) used here are such that the carriers populate only the lowest subband. Carrier confinement in the well and reduction in the effects of ionized impurities establish a strong electron-electron interaction in the QW structure. This strong interaction in energy and momentum exchanges favors[3] a heated drifted Fermi–Dirac distribution function having an electron temperature T_e and a drift momentum p_d, as revealed by the photoluminescent experiments.[4] In the presence of a high electric field $\mathbf{F}$ applied parallel to the interfacial planes, the carrier distribution function $f(\mathbf{k})$ in the well is thus written as

$$f(\mathbf{k}) = f_0(E) + \frac{\hbar p_d k}{m^*}\left(-\frac{\partial f_0}{\partial E}\right)\cos\theta, \tag{1}$$

where $f_0(E)$ is the Fermi–Dirac distribution function for the carriers, θ is the angle between $\mathbf{F}$ and 2D wave vector $\mathbf{k}$ of the carriers with energy E, m^* is the electronic effective mass, and $\hbar$ is Planck's constant divided by 2π.

The electron energy loss via the longitudinal optic (LO) phonons and the momentum losses via LO, acoustic, and ionized impurity modes of scattering are incorporated. The phonon spectra are modified in a QW,[5] but inclusion of bulk-mode phonons gives results agreeing with that obtained by considering both the confined mode and the interface phonons.[6,7] In the present calculations, we take bulk-like phonons to avoid unmanageably complicated expressions of the scattering rates for the full phonon structure without greatly sacrificing the accuracy of the results. Screening effects are small at the LO phonon frequency in the temperature range where polar coupling is dominant,[8,9] and thus screening is ignored for polar optic scattering. For acoustic and impurity scatterings, however, screening is included. In modulation doped systems, theoretical treatments of far remote impurity scattering are inadequate. However, with sufficiently thick spacer layers, the effect of far remote impurity scattering can be significantly reduced,[10] and so it is ignored here. The detailed expressions for the total scattering rate due to LO phonons can be found in Refs. 11 and 12, and the momentum relaxation times for acoustic and background impurity interactions in Refs. 13 and 14.

We assume that the electric field consists of a steady part F_0 and a small-signal ac component with amplitude F_1 and angular frequency ω. Thus

 0021-8979/95/78(1)/283/5/$6.00

$$F = F_0 + F_1 \sin \omega t. \tag{2}$$

In the presence of the electric field, the electron temperature and the drift momentum will also have similar components with the alternating ones generally differing in phase. Hence we can write

$$T_e = T_0 + T_{1r} \sin \omega t + T_{1i} \cos \omega t, \tag{3}$$

and

$$p_d = p_0 + p_{1r} \sin \omega t + p_{1i} \cos \omega t. \tag{4}$$

The energy and momentum conservation equations for the electrons are

$$\frac{ep_d F}{m^*} + \left\langle \frac{dE}{dt} \right\rangle_s = \frac{d}{dt} \langle E \rangle, \tag{5}$$

and

$$eF + \left\langle \frac{dp}{dt} \right\rangle_s = \frac{dp_d}{dt}, \tag{6}$$

where e is the electronic charge, and $-\langle dE/dt \rangle_s$ and $-\langle dp/dt \rangle_s$ are scattering-controlled average energy and momentum loss rates, respectively. In extreme degenerate systems, the average electron energy $\langle E \rangle$ is determined by the Fermi energy so that the right-hand side of Eq. (5) goes to zero.

Inserting Eqs. (3) and (4) into Eqs. (5) and (6) we retain the terms only up to the first order in the small-signal parts. The steady components and the coefficients of $\sin \omega t$ and $\cos \omega t$ terms on the two sides of the resulting equations are then equated. This gives

$$F_0 p_0 = g_1(T_0), \tag{7}$$

$$\frac{F_0}{p_0} = g_2(T_0), \tag{8}$$

$$\frac{F_0}{p_0} \frac{p_1}{F_1} - g_3(T_0) \frac{T_1}{F_1} = -1, \tag{9}$$

and

$$\left(g_2(T_0) + j \frac{\omega}{e} \right) \frac{p_1}{F1} + g_4(T_0) \frac{T_1}{F_1} = 1. \tag{10}$$

Here, $p_1 = p_{1r} + jp_{1i}$ and $T_1 = T_{1r} + jT_{1i}$ with $j^2 = -1$. The expressions for the functions $g_1(T_0)$ through $g_4(T_0)$ which depend on the distribution function and the scattering mechanisms, are relegated to the Appendix.

For a given T_0, Eqs. (7)–(10) can be solved for F_0, p_0, and p_1/F_1. The dc mobility μ_{dc} and the small-signal ac mobility μ_{ac} are given by

$$\mu_{dc} = \frac{p_0}{m^* F_0}, \tag{11}$$

and

TABLE I. Material parameters of GaAs.

Parameters	Values
Electron effective mass m^* (kg)	0.61033×10^{-31}
Longitudinal elastic constant, C_1 (N m^{-2})	14.03×10^{10}
Acoustic deformation potential, E_1 (J)	17.6×10^{-19}
Static dielectric constant, K_s	12.53
Optic dielectric constant, K_α	10.82
LO phonon angular frequency, ω_0 (rad s^{-1})	5.37×10^{13}

$$\mu_{ac} = \frac{|p_1|}{m^* F_1}. \tag{12}$$

The phase lag ϕ of the resulting alternating current behind the applied field is obtained from

$$\phi = \arctan\left(-\frac{p_{1i}}{p_{1r}} \right). \tag{13}$$

III. RESULTS AND DISCUSSIONS

Model calculations are performed with the parameter values of GaAs given in Table I for a bias field, $F_0 = 10^5$ V m^{-1}. A value of 11 eV for acoustic deformation potential E_1, as obtained from the analysis of energy loss rates of 2D electrons,[15] is used here instead of using the commonly accepted value of 7 eV.

Figure 1 shows the variation of μ_{ac}/μ_{dc} with frequency for $L = 10$ nm, $n_{2D} = 10^{16}$ m^{-2}, and ionized impurity concentration, $N_i = 6 \times 10^{21}$ m^{-3}. The values of μ_{dc} are calculated as 2.07 and 0.99 m^2 V^{-1} s^{-1} at 77 and 300 K, respectively. Although μ_{dc} is lower at 300 K than at 77 K due to the enhanced LO phonon scattering, μ_{ac}/μ_{dc} is found to be lower at 77 K due to more pronounced hot electron nonlinearity. The 3-dB cut-off frequency is 285 GHz for 77 K and 440 GHz for 300 K.

The frequency dependencies of the phase angle ϕ for the same parameters of Fig. 1 are depicted in Fig. 2. The angle ϕ

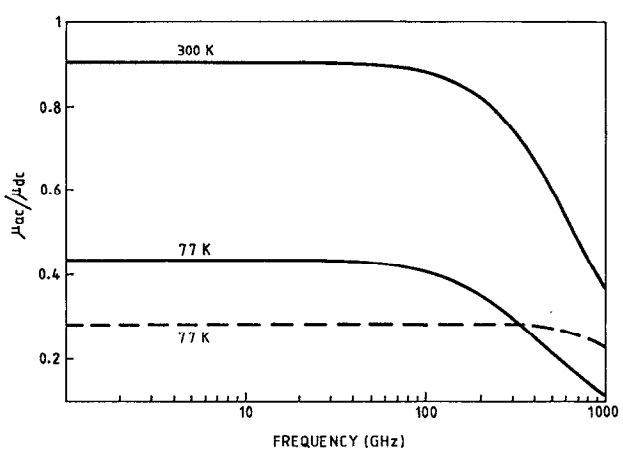

FIG. 1. Variation of μ_{ac}/μ_{dc} with frequency for 77 and 300 K. Solid curves are for $L = 10$ nm, $n_{2D} = 10^{16}$ m^{-2}, and $N_i = 10^{21}$ m^{-3}. The dashed curve is for a nondegenerate system with $L = 10$ nm (Ref. 16).

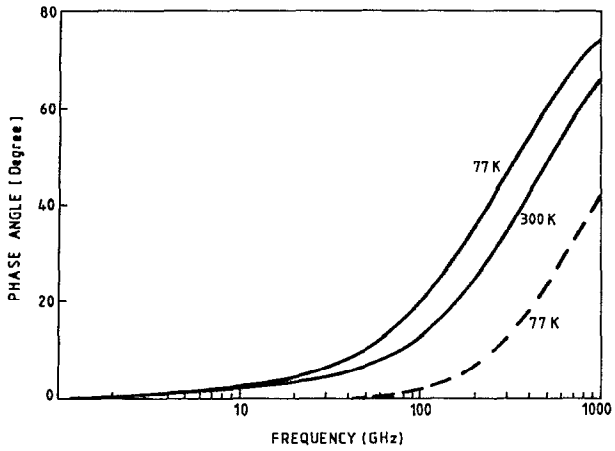

FIG. 2. Plot of the phase lag ϕ of the drift velocity behind the applied signal versus frequency for 77 and 300 K. The parameter values are the same and the solid and the dashed curves have the same significance as in Fig. 1.

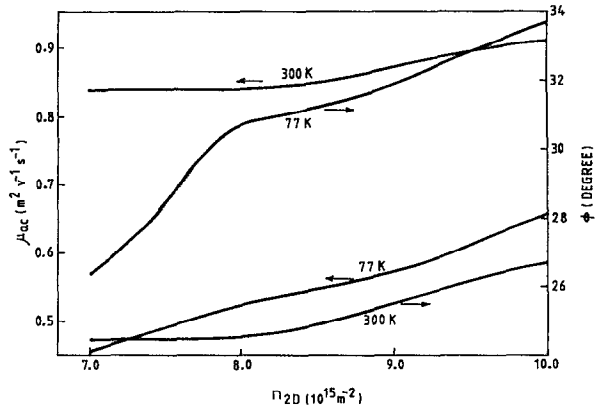

FIG. 4. Plot of μ_{ac} and ϕ with n_{2D} at 200 GHz for 77 and 300 K. The other parameters have the same values as in Fig. 1.

increases significantly beyond 30 GHz and is found to be higher at 77 K than at 300 K due to the reduced scattering at the former temperature.

The dashed curves in Figs. 1 and 2 give the results obtained in an earlier article[16] at 77 K for a nondegenerate system with a drifted Maxwellian distribution function. In Ref. 16, impurity scattering was ignored and the momentum conservation approximation (MCA)[17] was used. The value of μ_{ac} obtained in Ref. 16 is 1.39 $m^2 V^{-1} s^{-1}$ which is lower than the value of 2.07 $m^2 V^{-1} s^{-1}$ found in the present more realistic model where the system is taken to be degenerate, MCA is removed, and impurity scattering is included. The dashed curve in Fig. 1 shows that μ_{ac} begins to fall from about 350 GHz compared to 100 GHz revealed by the present calculation. Also the phase angle ϕ is found to be lower in Ref. 16. The high-frequency performance of 2D electron gas is thus overestimated in the simplified model of Ref. 16.

Figure 3 shows the channel width dependence of μ_{ac} and ϕ for 77 and 300 K at a frequency of 200 GHz, the other parameters remaining the same as in Fig. 1. The chosen frequency is sufficiently high for a departure from the low-frequency behavior. Both μ_{ac} and ϕ increase with increasing L owing to the reduced scattering for a higher channel width.[11]

The variation of μ_{ac} and ϕ with n_{2D} at 77 and 300 K at a frequency of 200 GHz is given in Fig. 4, the other parameters being the same as in Fig. 1. Both μ_{ac} and ϕ generally increase with n_{2D}. The weakening of scattering at higher n_{2D} due to enhanced screening and upward shift of the Fermi level (E_F) accounts for this behavior.

Figure 5 gives the plot of the 3 dB cut-off frequency $f_{3\ dB}$ versus the channel width L for 77 and 300 K with the $n_{2D}=8\times10^{15}$ and 10^{16} m^{-2}, the other parameters being identical to those of Fig. 1. $f_{3\ dB}$ is found to decrease with increasing L, reflecting that the fall of μ_{ac} with frequency is

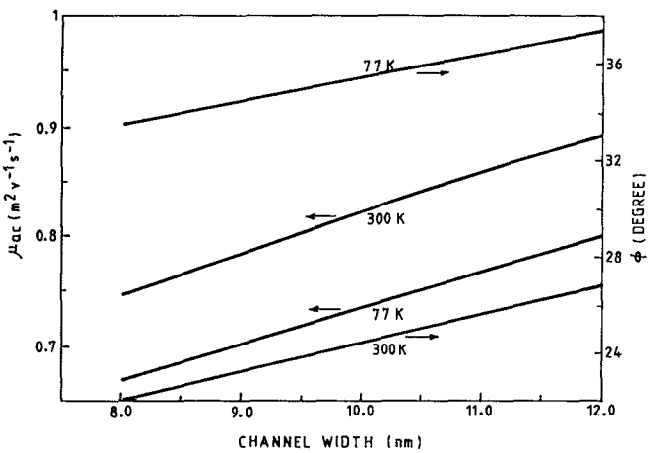

FIG. 3. Variation of μ_{ac} and ϕ with L at a frequency of 200 GHz for 77 and 300 K. The other parameters are the same as in Fig. 1.

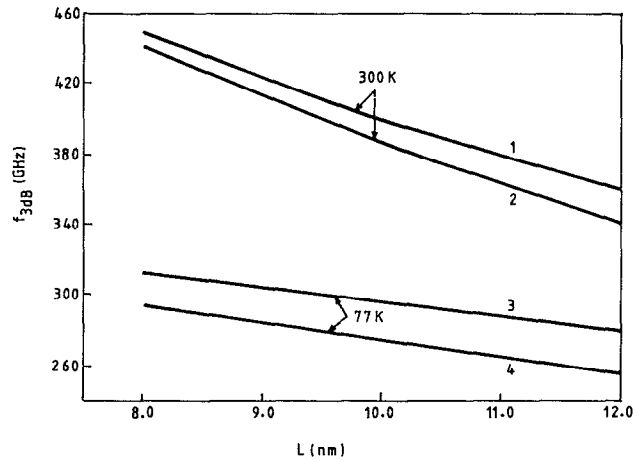

FIG. 5. Plot of the 3 dB cut-off frequency f_{3dB} vs the channel width L for 77 and 300 K. (1), (4): $n_{2D}=10^{16}$ m^{-2}; (2), (3): $n_{2D}=8\times10^{15}$ m^{-2}. The other parameters are identical to those of Fig. 1.

sharper at a greater value of L. The values of f_{3dB} are higher at 300 K than at 77 K, particularly for lower channel widths.

In conclusion, detailed calculations on the high-frequency behavior of hot electrons in a GaAs square QW are reported. We find that the high-frequency response is overestimated in the simplified model of Ref. 16. The dependencies of the ac mobility on various system parameters are presented and explained with our model. The results presented here give useful information on the performance of quantum structures in high-frequency devices.

ACKNOWLEDGMENT

P. K. Ghosh gratefully acknowledges the financial support rendered by the Council of Scientific and Industrial Research, India, in the form of Senior Research Fellowship.

APPENDIX

Expressions for the functions $g_i(T_0)$; $i=1,2,3,4$.

$$g_1(T_0)=A\left((N_0+1)\int_{\hbar\omega_0}^{\infty} I_2(E,T_0)f_{00}(E)[1-f_{00}(E-\hbar\omega_0)]dE-N_0\int_0^{\infty} I_1(E,T_0)f_{00}(E)[1-f_{00}(E+\hbar\omega_0)]dE\right),$$

$$g_2(T_0)=B\int_0^{\infty}\psi(E)f_{00}(E)[1-f_{00}(E)]E^{1/2}dE+C\int_0^{\infty}\lambda_1(E)f_{00}(E)[1-f_{00}(E)]EdE+D\left((N_0+1)\int_{\hbar\omega_0}^{\infty} I_2'(E,T_0)f_{00}(E)\right.$$
$$\left.\times[1-f_{00}(E)][1-f_{00}(E-\hbar\omega_0)]E^{1/2}dE-N_0\int_0^{\infty} I_1'(E,T_0)f_{00}(E)[1-f_{00}(E)][1-f_{00}(E+\hbar\omega_0)]E^{1/2}dE\right),$$

$$g_3(T_0)=\frac{A}{P_0T_0}\left\{(N_0+1)\int_{\hbar\omega_0}^{\infty} I_2(E,T_0)f_{00}(E)[1-f_{00}(E-\hbar\omega_0)]\left[[1-f_{00}(E)-f_{00}(E-\hbar\omega_0)]\left(\frac{E-E_F}{k_BT_0}\right)\right.\right.$$
$$\left.+\frac{\hbar\omega_0}{k_BT_0}f_{00}(E-\hbar\omega_0)\right]dE-N_0\int_0^{\infty} I_1(E,T_0)f_{00}(E)[1-f_{00}(E+\hbar\omega_0)]\left[[1-f_{00}(E)-f_{00}(E+\hbar\omega_0)]\left(\frac{E-E_F}{k_BT_0}\right)\right.$$
$$\left.\left.-\frac{\hbar\omega_0}{k_BT_0}f_{00}(E+\hbar\omega_0)\right]dE\right\},$$

$$g_4(T_0)=\frac{BP_0}{T_0}\int_0^{\infty}\psi(E)f_{00}(E)[1-f_{00}(E)]\left[[1-2f_{00}(E)]\left(\frac{E-E_F}{k_BT_0}\right)-1\right]E^{1/2}dE+\frac{CP_0}{T_0}\left\{(N_0+1)\int_0^{\infty}\lambda_1(E)f_{00}(E)\right.$$
$$\times[1-f_{00}(E)]\left[[1-2f_{00}(E)]\left(\frac{E-E_F}{k_BT_0}\right)-1\right]EdE+\frac{DP_0}{T_0}(N_0+1)\int_{\hbar\omega_0}^{\infty} I_2'(E,T_0)f_{00}(E)[1-f_{00}(E)][1-f_{00}(E$$
$$-\hbar\omega_0)]\left[[1-2f_{00}(E)-f_{00}(E-\hbar\omega_0)]\left(\frac{E-E_F}{k_BT_0}\right)+\frac{\hbar\omega_0}{k_BT_0}f_{00}(E-\hbar\omega_0)-1\right]E^{1/2}dE-N_0\int_0^{\infty} I_1'(E,T_0)f_{00}(E)$$
$$\left.\times[1-f_{00}(E)][1-f_{00}(E+\hbar\omega_0)]\left[[1-2f_{00}(E)-f_{00}(E+\hbar\omega_0)]\left(\frac{E-E_F}{k_BT_0}\right)-\frac{\hbar\omega_0}{k_BT_0}f_{00}(E+\hbar\omega_0)-1\right]E^{1/2}dE\right\}.$$

In the above expressions

$$I_1(E,T_0)=\int_0^{\pi}\frac{q_+^a(E,\phi)I_{2D}[q_+^a(E,\phi),L]}{\sqrt{(E/\hbar\omega_0)\cos^2\phi+1}}d\phi,$$

$$I_2(E,T_0)=\int_0^{\phi_{\max}}\frac{q_+^e(E,\phi)I_{2D}[q_+^e(E,\phi),L]+q_-^e(E,\phi)I_{2D}[q_-^e(E,\phi),L]}{\sqrt{(E/\hbar\omega_0)\cos^2\phi-1}}d\phi,$$

$$I_1'(E,T_0)=\int_0^{\pi}\cos\phi\,\frac{[q_+^a(E,\phi)]^2I_{2D}[q_+^a(E,\phi),L]}{\sqrt{(E/\hbar\omega_0)\cos^2\phi+1}}d\phi,$$

$$I_2'(E,T_0)=\int_0^{\phi_{\max}}\cos\phi\,\frac{[q_+^e(E,\phi)]^2I_{2D}[q_+^e(E,\phi),L]+[q_-^e(E,\phi)]^2I_{2D}[q_-^e(E,\phi),L]}{\sqrt{(E/\hbar\omega_0)\cos^2\phi-1}}d\phi.$$

$$\psi(E)=\frac{1}{\beta^2 E}\int_0^{2\beta\sqrt{E}}\frac{S^2(q)q^2}{\sqrt{1-q^2/(4\beta^2 E)}}\,dq,$$

$$\lambda_1(E)=\int_0^{\pi/2}\frac{x}{K^2}\left[\frac{6x^5}{\pi^4}+\frac{8x^3}{\pi^2}+\frac{1}{2}[1-\exp(-4x)]\right.$$
$$\left.-4[1-\exp(-2x)]\left(1+\frac{x}{2}+\frac{x^2}{x^2+\pi^2}\right)\right]$$
$$\times[4x^4+x^2(4\pi^2+3P)+2\pi^2 P]^{-2}d\theta,$$

$$A=\frac{m_0^{*^2}e\omega_0(K_s-K_\infty)}{8\pi^3\hbar^2 n_{2D}\epsilon_0 K_s K_\infty\sqrt{\hbar/(2m^*\omega_0)}},$$

$$B=\frac{3E_1^2 m^{*3/2}}{4\sqrt{2}\pi^2\hbar^4 C_1\, Ln_{2D}\, e}\frac{T_1}{T_0},$$

$$C=\frac{\pi^2 m^{*2}L^3 N_i e^3}{\epsilon_0^2 K_s^2 n_{2D} k_B\hbar^5 T_0},$$

$$D=\frac{e^2(K_s-K_\infty)m^{*1/2}}{8\sqrt{2}\pi^3\hbar^2\epsilon_0 K_s K_\infty n_{2D}k_B\sqrt{\hbar/(2m^*\omega_0)}}.$$

Here, $\beta=\sqrt{2m^*}/\hbar$, $f_{00}(E)$ is the Fermi–Dirac distribution function at temperature T_0 and N_0 denotes the phonon occupation number. T_1 represents the lattice temperature. ϵ_0 and k_B are the free-space permittivity and Boltzmann constant, respectively. The other symbols in the above expressions have been explained in Refs. 11 and 13.

[1] C. Weisbuch and B. Vinter, *Quantum Semiconductor Structures: Fundamentals and Applications* (Academic, New York, 1991), pp. 1–252.
[2] H. L. Störmer, J. Phys. Soc. Jpn. Suppl. A **49**, 1013 (1980).
[3] J. Shah, A. Pinczuk, A. C. Gossard, and W. Wiegmann, Phys. Rev. Lett. **54**, 2045 (1985).
[4] J. M. Carlson, S. A. Lyon, J. M. Worlock, A. C. Gossard, and W. Wiegmann, Bull. Amer. Phys. Soc. March Meeting, 1984, p. 213.
[5] M. Babiker and B. K. Ridley, Superlattices and Microstructures **2**, 287 (1986).
[6] N. Mori and T. Ando, Phys. Rev. B **40**, 6175 (1989).
[7] H. Rücker, E. Molinari, and P. Lugli, Phys. Rev. B **44**, 3463 (1991).
[8] X. L. Lei, J. Phys. C **18**, L593 (1985).
[9] P. J. Price, Phys. Rev. B **32**, 2643 (1985).
[10] J. J. Harris, C. T. Foxon, D. E. Lacklison, and K. W. J. Barnham, Superlattices and Microstructures **2**, 563 (1986).
[11] J. P. Leburton, J. Appl. Phys. **56**, 2850 (1984).
[12] D. Chattopadhyay, Phys. Rev. B **33**, 7288 (1986).
[13] D. Chattopadhyay, Phys. Status Solidi B **135**, 409 (1986).
[14] J. Lee, H. N. Spector, and V. K. Arora, J. Appl. Phys. **54**, 6995 (1983).
[15] K. Hirakawa and H. Sakaki, Appl. Phys. Lett. **49**, 889 (1986).
[16] A. Bhattacharya, A. Ghosal, and D. Chattopadhyay, Phys. Status Solidi B **127**, 427 (1985).
[17] B. K. Ridley, J. Phys. C **15**, 5899 (1982).